

Density functional theory for calculation of elastic properties of orthorhombic crystals: Application to TiSi_2

P. Ravindran,^{a)} Lars Fast, P. A. Korzhavyi, and B. Johansson
*Department of Physics, Condensed Matter Theory Group, Uppsala University, Box 530,
75121 Uppsala, Sweden*

J. Wills
*Theoretical Division, Los Alamos National Laboratory, Los Alamos,
New Mexico 87545*

O. Eriksson
*Department of Physics, Condensed Matter Theory Group, Uppsala University, Box 530, 75121 Uppsala,
Sweden, and Los Alamos National Laboratory, Los Alamos, New Mexico 87545*

(Received 8 June 1998; accepted for publication 31 July 1998)

A theoretical formalism to calculate the single crystal elastic constants for orthorhombic crystals from first principle calculations is described. This is applied for TiSi_2 and we calculate the elastic constants using a full potential linear muffin-tin orbital method using the local density approximation (LDA) and generalized gradient approximation (GGA). The calculated values compare favorably with recent experimental results. An expression to calculate the bulk modulus along crystallographic axes of single crystals, using elastic constants, has been derived. From this the calculated linear bulk moduli are found to be in good agreement with the experiments. The shear modulus, Young's modulus, and Poisson's ratio for ideal polycrystalline TiSi_2 are also calculated and compared with corresponding experimental values. The directional bulk modulus and the Young's modulus for single crystal TiSi_2 are estimated from the elastic constants obtained from LDA as well as GGA calculations and are compared with the experimental results. The shear anisotropic factors and anisotropy in the linear bulk modulus are obtained from the single crystal elastic constants. From the site and angular momentum decomposed density of states combined with a charge density analysis and the elastic anisotropies, the chemical bonding nature between the constituents in TiSi_2 is analyzed. The Debye temperature is calculated from the average elastic wave velocity obtained from shear and bulk modulus as well as the integration of elastic wave velocities in different directions of the single crystal. The calculated elastic properties are found to be in good agreement with experimental values when the generalized gradient approximation is used for the exchange and correlation potential. © 1998 American Institute of Physics.
[S0021-8979(98)03821-3]

I. INTRODUCTION

Elastic properties of a solid are important because they relate to various fundamental solid-state properties such as interatomic potentials, equation of state, and phonon spectra. Elastic properties are also linked thermodynamically to the specific heat, thermal expansion, Debye temperature, melting point, and Grüneisen parameter. Plastic properties of materials are also closely associated with the shear moduli along the slip planes of mobile dislocations, since these dislocations can dissociate into partials with a spacing determined by the balance between the fault energy and the repulsive elastic force. The elastic constants determine the response of the crystal to external forces, as characterized by bulk modulus, shear modulus, Young's modulus, and Poisson's ratio, and obviously play an important part in determining the strength of the materials. Values of elastic constants provide valuable information about the bonding characteristic between adjacent atomic planes and the anisotropic character of

the bonding and structural stability. It has also been noticed that there is a correlation between the elastic constants and the melting temperature of a solid.^{1,2} Pugh³ introduced the ratio between the bulk and shear modulus, B/G , for polycrystalline phases as a measure of fracture/toughness in metals. A high (low) B/G value is associated with ductility (brittleness), and we will elaborate on this empirical relationship later.

Elastic constants for most pure metals are available over a wide range of temperature in the literature. In contrast, data for alloys and intermetallic compounds are much more limited. In particular, single crystal elastic constants, which are required in the basic studies mentioned above, are not available except for a few intermetallic compounds.⁴ Efforts have been made to calculate the elastic constants theoretically from so-called first principles calculations and, although the bulk modulus has been calculated for various materials, calculations of the other elastic constants are relatively scarce.⁵ Among these most of the attempts have been made to calculate the elastic constants of cubic materials⁶ from first prin-

^{a)}Electronic mail: P.Ravindran@fysik.uu.se

ciples, while only very few have been made to calculate the elastic constants of low symmetry systems such as tetragonal⁷ and hexagonal⁸ systems. The main problem in estimating elastic constants from first principles is not only the requirement of accurate methods for calculating the total energy but also the complicated heavy computations involved in the calculation of elastic constants. Further, if the symmetry of the system is reduced, the number of independent elastic constants increases and hence a larger number of distortions is required to calculate the full set of elastic constants. Because of the above facts no attempt has, to our knowledge, yet been made to calculate the elastic constants of low symmetric systems with orthorhombic, monoclinic, and triclinic structures.

The elastic behavior of a completely asymmetric material is specified by 21 independent elastic constants, while for an isotropic material, the number is 2. In between these limits the necessary number is determined by the symmetry of the material, and it is 9 for orthorhombic crystals. These nine independent elastic constants are usually referred to as C_{11} , C_{22} , C_{33} , C_{44} , C_{55} , C_{66} , C_{12} , C_{13} , and C_{23} . A theoretical treatment of the elasticity of orthorhombic systems is thus considerably more involved than for cubic, hexagonal, and tetragonal structures which have three, five, and six independent elastic constants, respectively. The task of calculating the elastic constants of orthorhombic crystals becomes even more difficult when realizing that the strains needed to calculate some of them give rise to a geometry with very low symmetry. Possibly this is the reason why so far no theoretical work on elastic constants of orthorhombic systems based on first principle methods have been published.

Titanium silicides, with their distinct properties of low density, high thermal and electrical conductivity, strong adhesion with silicon substrates, and high corrosion resistance to caustic gases, are mainly applied in very large scale integration (VLSI) circuits, such as interconnects, gate metallization, and Schottky barriers. Further, the low density, high creep strength, high melting point, superior oxidation resistance, high hardness (≈ 850 Hv), and flow stresses of more than 1200 MPa for TiSi_2 makes this compound a potential aero-space engineering material. All nine independent elastic constants of the orthorhombic C54 structure TiSi_2 have recently been determined experimentally.² This motivated us to calculate all nine independent elastic constants and related properties of TiSi_2 from first principle electronic structure calculations. Because of the special significance of the isotropic bulk modulus, shear modulus, Young's modulus, and Poisson's ratio for technological and engineering applications, we have also calculated these quantities from the elastic constants.

The remainder of the paper is organized as follows: In Sec. II we describe the underlying theory for the calculation of elastic constants of orthorhombic crystals as well as the computational aspects of our study. In Sec. III we have compared our theoretically obtained single crystal elastic constant data with the experiment. Section IV deals with the polycrystalline bulk modulus, shear modulus, Young's modulus, and Poisson's ratio, using the single crystal elastic constants obtained from our present numerical work, as well as

TABLE I. The equilibrium structural parameters for TiSi_2 obtained from the LDA and GGA calculations. The lattice parameters a , b , and c are in \AA and the equilibrium unit cell volume (V_0) is in \AA^3 .

	a	b	c	a/b	c/b	V_0
LDA	8.08	4.74	8.53	1.71	1.80	326.74
GGA	8.21	4.81	8.64	1.71	1.80	340.95
Experiment ^a	8.27	4.80	8.55	1.72	1.78	339.30

^aFrom Ref. 11.

those reported from the experimental studies. In Sec. V we discuss the elastic anisotropy in TiSi_2 through shear anisotropy factors, bulk modulus anisotropic factor, and percentage elastic anisotropy. In Sec. VI the nature of chemical bonding in TiSi_2 has been investigated through the elastic anisotropy, site and angular momentum decomposed density of state (DOS), and charge density analysis. In Sec. VII we have calculated the Debye temperature from the elastic constants by using the average elastic wave velocity as well as the integration of elastic wave velocity in a different direction of the single crystal. The important conclusions derived from our calculations are summarized in Sec. VIII. The explicit expressions to calculate bulk modulus along crystallographic directions from elastic constants for orthorhombic crystals as well as the calculated values are given in the Appendix.

II. DETAILS OF CALCULATIONS

A. Crystal structure aspects of TiSi_2

TiSi_2 crystallizes in the C54 type of structure (space group $Fddd D_{2h}^{24}$) congruently at 1480 °C from the melt and the room temperature lattice parameters are presented in Table I. There are 16 silicon and eight titanium atoms in the unit cell at $16e$ ($1/3$ 0 0) and $8a$ (0 0 0) Wyckoff positions, respectively. The crystal structure of TiSi_2 in the C54 (OF24) structure is shown in Fig. 1. In this figure the titanium and silicon as well as silicon and silicon are connected by bonds. The unit cell of TiSi_2 contains 24 atoms or eight formula units with close-packed hexagonal layers, which are stacked on top of each other in such a way that the Ti atoms of adjacent layers avoid close contact.⁹ In the transition metal disilicides with C11_b (MoSi_2) and C40 (CrSi_2 , NbSi_2 and TaSi_2) structures, the silicon atoms remain closely

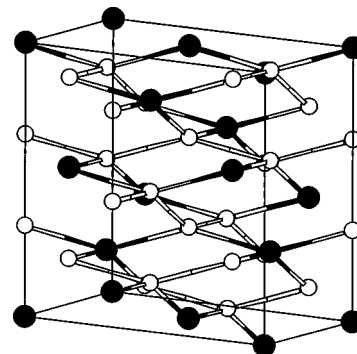


FIG. 1. The C54 type crystal structure of TiSi_2 . The black balls represent the Ti atoms and the white balls represent Si atoms.

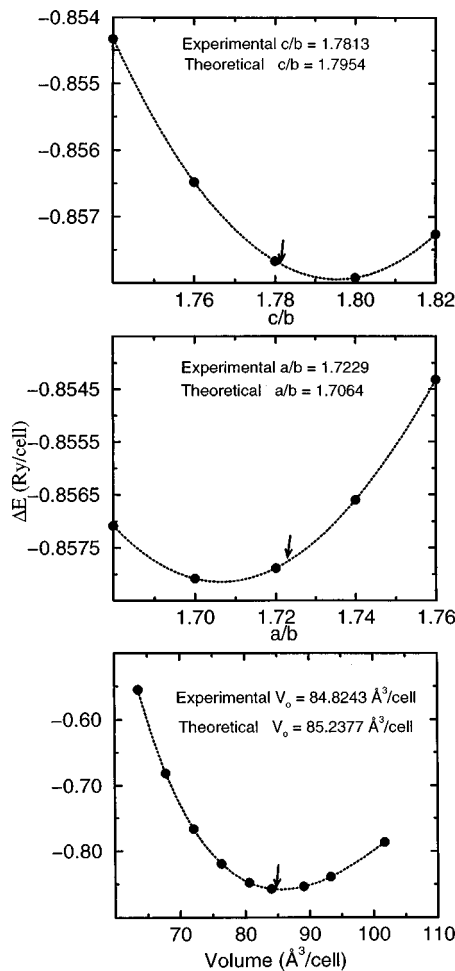


FIG. 2. The structural optimization curves for TiSi₂ from GGA calculations. The experimental structural parameters are taken from Rosenkranz and Frommeyer (see Ref. 11) ΔE represent the total energy added by 5737 Ry/cell.

bonded in sheets normal to the stacking plane.¹⁰ However, for the C54 (TiSi₂) structure, the Si–Si chain is interrupted with Ti atoms as shown in Fig. 1. The breaking of the Si–Si chains qualitatively implies increased metallic character and this may be the reason for the elevated thermal and electrical conductivity in TiSi₂, among the transition metal disilicides.

B. Structural optimization from total energy studies

Before performing calculations to obtain the elastic constants we have first optimized the structural parameters of TiSi₂ using both the local density approximation (LDA) as well as the generalized gradient approximation (GGA). In doing this we first adopted the experimental *a/b* and *c/b* ratios and optimized the equilibrium volume. We then used the theoretical equilibrium volume and optimized the ratio *a/b* as well as *c/b*. The structural optimization, total energy curves for TiSi₂ obtained from our GGA calculations are shown in Fig. 2. From this figure it is clear that the equilibrium structural parameters obtained from our GGA calculations are in very good agreement with the corresponding experimental values.

In Table I we list the calculated and experimental values of the equilibrium lattice parameters and volume obtained

from our LDA as well as GGA calculations along with the experimental values.¹¹ The theoretically estimated equilibrium volume, which neglects zero-point motion and thermal expansion, is underestimated in our LDA calculation by 3.7%, relative to the experimental value and **overestimated by 0.5% in our GGA calculation.** From Table I we have thus found that overall the equilibrium lattice parameters obtained from our GGA calculations are in better agreement with the experiments than those obtained from our LDA calculations.

C. Calculation of elastic constants

The face centered orthorhombic phase of TiSi₂ has three lattice parameters *a*, *b*, and *c*, with the Bravais lattice vectors of the matrix form

$$R = 1/2 \begin{pmatrix} 0 & 1 & c/b \\ a/b & 0 & c/b \\ a/b & 1 & 0 \end{pmatrix}.$$

The full potential linearized muffin-tin orbital (FPLMTO)¹² method allows total energy calculations to be done for arbitrary crystal structures. **We can therefore apply small strains to the equilibrium lattice, determine the resulting change in the total energy, and from this information deduce the elastic constants.** The elastic constants are identified as proportional to the second order coefficient in a polynomial fit of the total energy as a function of the distortion parameter δ.¹³ We determine linear combinations of the elastic constants by straining the lattice vectors **R** according to the rule **R'** = **RD**. Here **R'** is a matrix containing the components of the distorted lattice vectors and **D** is the symmetric distortion matrix, which contains the strain components. We shall consider only small lattice distortions in order to remain within the elastic limit of the crystal. In the following we shall briefly list the relevant formulas needed to obtain the elastic constants of orthorhombic crystals. **The internal energy of a crystal under strain, δ, can be Taylor expanded** in powers of the strain tensor with respect to the initial internal energy of the unstrained crystal in the following way:

$$E(V, \delta) = E(V_0, 0) + V_0 \left(\sum_i \tau_i \xi_i \delta_i + 1/2 \sum_{ij} c_{ij} \delta_i \xi_i \delta_j \xi_j \right) + O(\delta^3). \quad (1)$$

The volume of the unstrained system is denoted *V*₀ and *E*(*V*₀, 0) is the corresponding total energy. We have used the Voigt notation in the equation above which replaces *xx*, *yy*, *zz*, *yz*, *xz*, and *xy* by 1, 2, 3, 4, 5, and 6, respectively. When introducing the Voigt notation, one has to remember that the δ's are symmetric. To account for this, we introduced the factor ξ_{*i*}, which takes the value 1 if the Voigt index is 1, 2, or 3 and the value 2 if the Voigt number is 4, 5, or 6. In the equation above, τ_{*i*} is an element in the stress tensor. The Taylor expansion of the total energy should be done in terms of Lagrangian coordinates **η** which relate the Eulerian coordinates **δ** by the equation, **η** = **δ** + ½ **δδ**. Since **δ** is small the approximation **η** = **δ** is valid (the effect in the present case is the third decimal).

Since we have nine independent elastic constants, we need nine different strains to determine these. The nine distortions used in the present investigation are described below. The first three elastic constants, c_{11} , c_{22} , and c_{33} , are obtained by the following distortion matrices D_1 , D_2 , and D_3 , respectively, and correspond to straining the lattice along the x , y , and z axis, respectively. These distortion matrices are written as

$$D_1 = \begin{pmatrix} 1 + \delta & 0 & 0 \\ 0 & 1 & 0 \\ 0 & 0 & 1 \end{pmatrix},$$

$$D_2 = \begin{pmatrix} 1 & 0 & 0 \\ 0 & 1 + \delta & 0 \\ 0 & 0 & 1 \end{pmatrix}$$

and

$$D_3 = \begin{pmatrix} 1 & 0 & 0 \\ 0 & 1 & 0 \\ 0 & 0 & 1 + \delta \end{pmatrix}.$$

In all these distortions, the symmetry of the strained lattice still remains orthorhombic. However, the volume is changed by the distortion. The energy associated with these distortions can be obtained by putting the values of the strain matrices D_1 , D_2 , and D_3 in Eq. (1) and we obtain

$$E(V, \delta) = E(V_0, 0) + V_0 \left(\tau_1 \delta + \frac{c_{11}}{2} \delta^2 \right), \tag{2}$$

$$E(V, \delta) = E(V_0, 0) + V_0 \left(\tau_2 \delta + \frac{c_{22}}{2} \delta^2 \right), \tag{3}$$

and

$$E(V, \delta) = E(V_0, 0) + V_0 \left(\tau_3 \delta + \frac{c_{33}}{2} \delta^2 \right), \tag{4}$$

respectively. From these relations we obtain the elastic constants c_{11} , c_{22} , and c_{33} . Using the following volume conserving monoclinic shear distortions,

$$D_4 = \begin{pmatrix} \frac{1}{(1-\delta^2)^{1/3}} & 0 & 0 \\ 0 & \frac{1}{(1-\delta^2)^{1/3}} & \frac{\delta}{(1-\delta^2)^{1/3}} \\ 0 & \frac{\delta}{(1-\delta^2)^{1/3}} & \frac{1}{(1-\delta^2)^{1/3}} \end{pmatrix},$$

$$D_5 = \begin{pmatrix} \frac{1}{(1-\delta^2)^{1/3}} & 0 & \frac{\delta}{(1-\delta^2)^{1/3}} \\ 0 & \frac{1}{(1-\delta^2)^{1/3}} & 0 \\ \frac{\delta}{(1-\delta^2)^{1/3}} & 0 & \frac{1}{(1-\delta^2)^{1/3}} \end{pmatrix}$$

and

$$D_6 = \begin{pmatrix} 1 & \delta & 0 \\ \frac{\delta}{(1-\delta^2)^{1/3}} & \frac{1}{(1-\delta^2)^{1/3}} & 0 \\ 0 & 0 & \frac{1}{(1-\delta^2)^{1/3}} \end{pmatrix},$$

we obtain the shear elastic constants c_{44} , c_{55} , and c_{66} . The energy corresponding to the distortions D_4 , D_5 , and D_6 can be written as

$$E(V, \delta) = E(V_0, 0) + V_0 (2\tau_4 \delta + 2c_{44} \delta^2), \tag{5}$$

$$E(V, \delta) = E(V_0, 0) + V_0 (2\tau_5 \delta + 2c_{55} \delta^2), \tag{6}$$

and

$$E(V, \delta) = E(V_0, 0) + V_0 (2\tau_6 \delta + 2c_{66} \delta^2), \tag{7}$$

respectively. The relations above give the c_{44} , c_{55} , and c_{66} elastic constants directly. We are left with three more elastic constants c_{12} , c_{13} , and c_{23} . These elastic constants can be calculated by means of volume conserving orthorhombic distortions of the following types:

$$D_7 = \begin{pmatrix} \frac{1+\delta}{(1-\delta^2)^{1/3}} & 0 & 0 \\ 0 & \frac{1-\delta}{(1-\delta^2)^{1/3}} & 0 \\ 0 & 0 & \frac{1}{(1-\delta^2)^{1/3}} \end{pmatrix},$$

$$D_8 = \begin{pmatrix} \frac{1+\delta}{(1-\delta^2)^{1/3}} & 0 & 0 \\ 0 & \frac{1}{(1-\delta^2)^{1/3}} & 0 \\ 0 & 0 & \frac{1-\delta}{(1-\delta^2)^{1/3}} \end{pmatrix}$$

and

$$D_9 = \begin{pmatrix} \frac{1}{(1-\delta^2)^{1/3}} & 0 & 0 \\ 0 & \frac{1+\delta}{(1+\delta^2)^{1/3}} & 0 \\ 0 & 0 & \frac{1-\delta}{(1-\delta^2)^{1/3}} \end{pmatrix}.$$

Among these three distortions, D_7 increases a and decreases b with an equal amount and c remains constant. The D_8 distortion increases a and decreases c with an equal amount and b is kept constant. The D_9 distortion, finally increases b and decreases c with an equal amount and a remains constant. Hence, the resulting symmetry of the strained object from the D_7 , D_8 , and D_9 distortions is the same as that of the unstrained lattice and in addition the volume is conserved in these distortions.

The energy associated with these distortions can be obtained by putting the values of the strain matrices D_7 , D_8 , and D_9 into Eq. (1) and are

$$E(V, \delta) = E(V_0, 0) + V_0[(\tau_1 - \tau_2)\delta + \frac{1}{2}(c_{11} + c_{22} - 2c_{12})\delta^2], \quad (8)$$

$$E(V, \delta) = E(V_0, 0) + V_0[(\tau_1 - \tau_3)\delta + \frac{1}{2}(c_{11} + c_{33} - 2c_{13})\delta^2], \quad (9)$$

and

$$E(V, \delta) = E(V_0, 0) + V_0[(\tau_2 - \tau_3)\delta + \frac{1}{2}(c_{22} + c_{33} - 2c_{23})\delta^2], \quad (10)$$

respectively. The relations above give the value of the elastic constants c_{12} , c_{13} , and c_{23} with the superposition of the already calculated elastic constants c_{11} , c_{22} , and c_{33} .

D. Computational details

Using the above-mentioned strains, we have calculated the total energy self-consistently by means of first principles electronic structure calculations, based on the density-functional theory and we use the all-electron full potential linear muffin-tin orbital method.¹² The calculations of the elastic constants were done at the theoretically derived equilibrium lattice parameters. In the FPLMTO method, no shape approximation is made to the potential and the charge density; the warping terms in the interstitial region and the non-spherical contribution at the sites of the nuclei are explicitly taken into account. The density and potential are expanded in cubic harmonics inside non-overlapping muffin-tin (MT) spheres and in a Fourier series in the interstitial region. The ratio between the lattice constant a and the muffin-tin radius was kept constant for the various strains and was chosen to be equal for both the Ti and Si MT spheres. Spherical harmonic expansions were carried out through $l_{\max}=8$ for the bases, potential, and charge density. The exchange and correlation potential was treated in the LDA using the von Barth-Hedin parametrization. The LDA is in principle only valid for slowly varying densities and is known to show an overbinding of atoms in molecules and solids. Hence, to remedy this situation we have also used the GGA as proposed by Perdew and Wang.¹⁴

The basis set was comprised of augmented linear muffin-tin orbitals.¹⁵ The tails of the basis functions outside their parent spheres were linear combinations of Hankel or Neumann functions with nonzero kinetic energy. The basis contains $4s$, $3p$, $5p$, $3d$, and $4f$ orbitals on the titanium site and $3s$, $2p$, $3p$, $3d$, and $4f$ for the Si site. All orbitals were contained in the same energy panel, with the $3p$ of Ti and $2p$ of Si treated as pseudovalence states in an energy set which is different from the rest of the basis function. Further, we used a so-called "double basis" where we used two different orbitals of l , m_l character each connecting, in a continuous and differential way, to Hankel or Neumann functions with different kinetic energy. The integration over the Brillouin zone was done using the special point sampling¹⁶ with a Gaussian width of ~ 10 mRy. For the calculations of

the equilibrium volume, a/b , c/b , and the strains D_1 , D_2 , D_3 , D_7 , D_8 , and D_9 , we have used 64 k points in the irreducible wedge of the first Brillouine zone (IBZ) of the face centered orthorhombic lattice. As mentioned earlier, the application of the D_4 , D_5 , and D_6 strains on the lattice implies a lowering of symmetry and hence we have used 100 k points in the IBZ of the primitive monoclinic lattice for these strains. **To avoid the influence of higher order terms on the estimated elastic constants we have used very small strains, i.e., within $\pm 1.5\%$.**

III. COMPARISON OF SINGLE CRYSTAL ELASTIC CONSTANTS

In Figs. 3(a) and 3(b) we have plotted the changes in total energy (ΔE) versus strain δ for TiSi_2 for the nine different types of distortions discussed in Sec. II C. The results are obtained from LDA and GGA calculations, respectively, using the corresponding theoretical equilibrium structural parameters given in Table I. The elastic constants c_{ij} are obtained by means of polynomial fits. The polynomial fit to the points [dotted lines in Figs. 3(a) and 3(b)] were truncated after the third-order term. It should be noted that, to minimize the errors coming from higher order terms, we have used very small distortions. We may now compare our calculated elastic constants with the experimental elastic constants measured at room temperature.² The elastic constants obtained from our GGA calculations given in Table II are found to compare very favorably with the experimental values, and are in somewhat better agreement with the experiment than the ones obtained from LDA calculations. The deviations in the calculated elastic constants from the experimental values are partly due to temperature and volume effects. It should also be noted that the elastic constants c_{12} , c_{13} , and c_{23} obtained both from LDA and GGA calculations deviate $\sim 25\%$ from the corresponding experimental values and one possible reason is as follows. The above-mentioned elastic constants are not possible to calculate straight away from just one single distortion, but can only be obtained together with other elastic constants. As an example c_{12} must thus be calculated from distortions D_1 , D_2 , and D_8 . From the corresponding equations (2), (3), and (8) we see that in order to extract c_{12} , we must subtract the second-order coefficient in the three equations from each other. However, errors made in calculating the different c_{ij} 's which were used to calculate the c_{12} may contribute to the error in c_{12} , producing a large deviation from the experiment. Hence, it is more reasonable to compare the appropriate superpositions of elastic constants rather than individual constants. As mentioned earlier the superposition of elastic constants $c_{11} + c_{22} - 2c_{12}$, $c_{11} + c_{33} - 2c_{13}$, and $c_{22} + c_{33} - 2c_{23}$ can be obtained directly from the D_7 , D_8 , and D_9 distortions, respectively. Hence, we compare these values with the experiment in Table II. It is interesting to note that the deviation between experiment and theory is drastically reduced when we compare the superposition of elastic constants rather than the individual values. Hence, we conclude that for TiSi_2 the

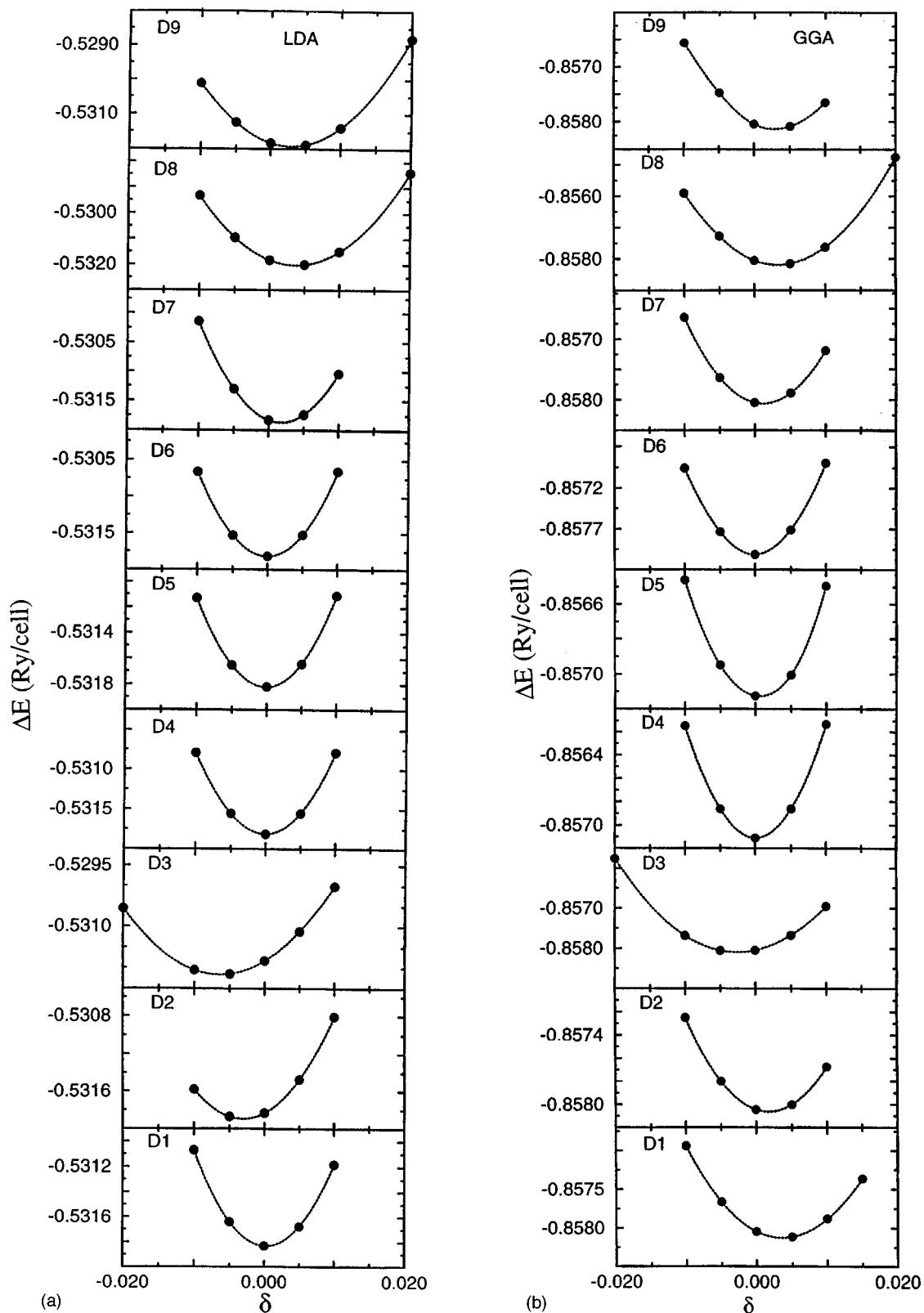


FIG. 3. Changes in the strain energy (ΔE) as a function of strain (δ) for TiSi_2 from LDA (a) and GGA (b) calculations. The black circles represent the calculated values and the dotted line is the polynomial fit. The arrows indicate the experimental values. ΔE represent the total energy added by 5737 Ry/cell.

deviation in elastic constants from the experimental values is within $\sim 30\%$ in the LDA calculations and within $\sim 18\%$ in our GGA calculation.

It is interesting to know the curvature of the total energy

with respect to length changes in any arbitrary direction. From the compliance constants it is possible to calculate this property, which is related to the directional bulk modulus K , using the following relation:

TABLE II. The single crystal elastic constants (c_{ij} in Mbar) for TiSi_2 obtained from LDA as well as GGA calculations. δ_L and δ_G are the percentage of deviation of elastic constants obtained from the LDA and GGA calculations from the experimental values.

c_{ij}	LDA	$\delta_L(\%)$	GGA	$\delta_G(\%)$	Exp ^a
c_{11}	3.772	18.8	3.260	2.6	3.175
c_{22}	3.411	6.4	2.984	-6.8	3.204
c_{33}	4.253	2.9	3.719	-9.9	4.132
c_{44}	1.365	21.3	1.235	9.7	1.125
c_{55}	0.937	23.6	0.853	12.5	0.758
c_{66}	1.546	31.5	1.359	15.7	1.175
c_{12}	0.278	5.3	0.224	23.7	0.293
c_{13}	0.213	-44.5	0.265	31.1	0.384
c_{23}	0.951	10.5	1.055	22.6	0.860
$c_{11} + c_{22} - 2c_{12}$	6.628	14.4	5.797	0.0	5.792
$c_{11} + c_{33} - 2c_{13}$	7.599	16.2	6.449	-1.3	6.538
$c_{22} + c_{33} - 2c_{23}$	5.763	2.6	4.593	18.2	5.616

^aFrom Nakamura (see Ref. 2).

$$\frac{1}{K} = (s_{11} + s_{12} + s_{13})l_1^2 + (s_{12} + s_{22} + s_{23})l_2^2 + (s_{13} + s_{23} + s_{33})l_3^2, \quad (11)$$

where l_1 , l_2 , and l_3 are the direction cosines. Using the above relation, the calculated bulk modulus along different directions from the theoretical as well as experimental elastic constants are shown in Fig. 4. For an isotropic system we will obtain a spherical shape in the directional dependent bulk modulus. The nonspherical nature of the bulk modulus of TiSi_2 in Fig. 4 clearly shows the anisotropy in the bulk modulus. To compare our theoretically obtained bulk modulus along different directions with experimental values one might add that if we compensate for the volume effect of the elastic constants we cannot conclude that the GGA calculations are better than the LDA calculations, but they are of the same magnitude. One way of compensating for the volume effect is to normalize the elastic constants with the corresponding bulk modulus.⁸ We have plotted the bulk modulus in different crystallographic planes in Fig. 5. From Fig. 5 it can be clearly seen that the bulk modulus obtained from the GGA calculation is in good agreement with the experiment regarding both the magnitude and directional behavior. We have also calculated the bulk modulus along the **a**, **b**, and **c** axes in Fig. 5. The calculated bulk modulus along the **a**, **b**, and **c** axes of TiSi_2 are consistent with the ones obtained

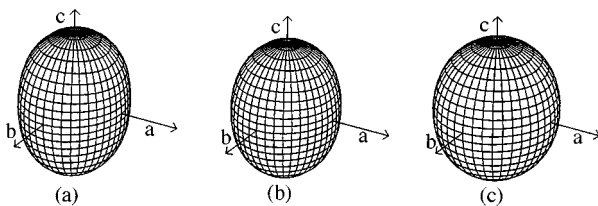


FIG. 4. Illustration of directional dependence of the bulk modulus. The distance between zero and any point on the ellipsoid/surface is equal to the bulk modulus in that direction: (a) calculated from LDA elastic constants, (b) from GGA elastic constants, and (c) from the experimental elastic constants of Nakamura (see Ref. 2) ΔE represent the total energy added by 5737 Ry/cell.

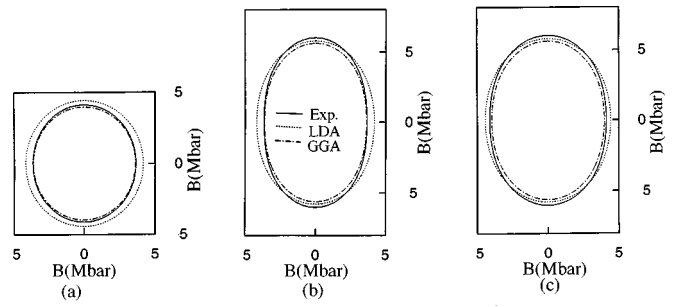


FIG. 5. The projections in different planes of the directional dependent bulk modulus for TiSi_2 . The continuous lines are obtained from the experimental bulk modulus of Nakamura (see Ref. 2); the dot dashed line represents the GGA results and the dotted line represents the LDA result: (a) along the *ab* plane, (b) along the *ac* plane, and (c) along the *bc* plane.

from experiments of the linear compressibility,¹⁷ where the change in the *a*, *b*, and *c* lattice parameters is measured as a function of hydrostatic pressure. The relationship between the linear compressibility and the elastic constants is derived in the Appendix and is given by Eqs. (A2)–(A4).

IV. CALCULATION OF ELASTIC CONSTANTS FOR POLYCRYSTALLINE AGGREGATES

A problem arises when single crystal samples are not available, since it is then not possible to measure the individual elastic constants c_{ij} . Instead, the polycrystalline bulk modulus (*B*) and shear modulus (*G*) may be determined. Consider a crystalline aggregate of single phase monocrystals having random orientation. The determination of the stress or strain distribution in the assemblage of such a polycrystalline aggregate with respect to an external load can be established for two extreme cases: that is, by equating either the uniform strain in the polycrystalline aggregate to the external strain or alternatively the uniform stress to the external stress. The former scheme is called the Voigt approximation¹⁸ and the latter is called the Reuss approximation.¹⁹ It is evident that the Voigt and Reuss assumptions are true only when the aggregate concerned is made up from isotropic crystals. If one is to calculate the average isotropic elastic moduli from the anisotropic single crystal elastic constants, one finds that the Voigt and Reuss assumptions result in the theoretical maximum and the minimum values of the isotropic elastic moduli, respectively. For specific cases of orthorhombic lattices, the Reuss shear modulus (G_R) and the Voigt shear modulus G_V are

$$G_R = \frac{15}{4(s_{11} + s_{22} + s_{33}) - 4(s_{12} + s_{13} + s_{23}) + 3(s_{44} + s_{55} + s_{66})}, \quad (12)$$

and

$$G_V = \frac{1}{15}(c_{11} + c_{22} + c_{33} - c_{12} - c_{13} - c_{23}) + \frac{1}{5}(c_{44} + c_{55} + c_{66}), \quad (13)$$

and the Reuss bulk modulus (B_R) and the Voigt bulk modulus (B_V) are defined as

TABLE III. The isotropic bulk modulus (B in Mbar) and shear modulus (G in Mbar) for polycrystalline TiSi_2 obtained from the single crystal elastic constants using Voigt, Reuss and Hill's approximations. The Young's modulus (E in Mbar) and the Poisson's ratio (ν) are estimated from Hill's approximation.

	B_R	B_V	B_H	G_R	G_V	G_H	E	ν
LDA	1.569	1.591	1.581	1.357	1.436	1.396	3.236	0.159
GGA	1.419	1.450	1.435	1.187	1.258	1.219	2.849	0.169
Exp ^a	1.468	1.509	1.489	1.129	1.209	1.169	2.781	0.188
Exp ^b	1.26	1.031	2.556	0.24
Ti	1.073	0.434	1.146	0.322
Si	0.988	0.663	1.625	0.226

^aCalculated from the single crystal elastic constants of M. Nakamura (see Ref. 2).

^bPolycrystalline measurements by Rosenkranz and Frommyer (see Ref. 11).

$$B_R = \frac{1}{(s_{11} + s_{22} + s_{33}) + 2(s_{12} + s_{13} + s_{23})}, \quad (14)$$

and

$$B_V = \frac{1}{9}(c_{11} + c_{22} + c_{33}) + \frac{2}{9}(c_{12} + c_{13} + c_{23}). \quad (15)$$

In Eqs. (12) and (14), the s_{ij} are the elastic compliance constants. Using energy considerations Hill²⁰ proved that the Voigt and Reuss equations represent upper and lower limits of the true polycrystalline constants, and recommended that a practical estimate of the bulk and shear moduli were the arithmetic means of the extremes. Hence, the elastic moduli of the polycrystalline material can be approximated by Hill's average and for shear moduli it is $G = \frac{1}{2}(G_R + G_V)$ and for bulk moduli it is $B = \frac{1}{2}(B_R + B_V)$.

The Young's modulus, E , and Poisson's ratio, ν , for an isotropic material are given by

$$E = \frac{9BG}{3B+G} \quad \text{and} \quad \nu = \frac{3B-2G}{2(3B+G)}, \quad (16)$$

respectively. Using the relations above the calculated bulk modulus, B , shear modulus, G , Young's modulus, E , and Poisson's ratio for TiSi_2 are given in Table III. In general the large value of shear moduli is an indication of the more pronounced directional bonding between atoms. The calculated shear moduli from LDA, GGA, and experimental single crystal elastic constants are larger than that of most of the intermetallic compounds.⁴ The somewhat larger value of G obtained from the LDA calculation compared to the GGA results indicates that LDA treats the bonding behavior of TiSi_2 slightly more directional than GGA. The factor that measures the stability of a crystal against shear is the Poisson's ratio. Our calculated Poisson's ratio is given in Table III for TiSi_2 and is considerably smaller than the values reported for most of the intermetallic compounds.⁴ The smaller value of Poisson's ratio indicates that TiSi_2 is relatively stable against shear. Pugh³ introduced the quotient of bulk to shear modulus of polycrystalline phases (B/G) by considering that the shear modulus G represents the resistance to plastic deformation, while the bulk modulus B represents the resistance to fracture. A high (low) B/G value is associated with ductility (brittleness). The critical value which separates ductile and brittle materials is about 1.75. It is interesting to try to understand the microscopic origin of this empirical parameter. Let us assume an isotropic cubic crystal and for

which the Cauchy relations $c_{11} = 3c_{12}$ and $c_{44} = c_{12}$ are valid. Hence the bulk modulus and shear modulus are reduced to

$$B = \frac{1}{3}(c_{11} + 2c_{12}) = \frac{5}{9}c_{11},$$

and

$$G = \begin{cases} c_{44} \\ \frac{1}{2}(c_{11} - c_{12}) \end{cases} = \frac{c_{11}}{3}.$$

From the above relations we can arrive the B/G value of 1.67. Although this parameter is mostly applied for cubic materials, it is interesting to examine TiSi_2 . The B/G value for the ductile Ti is 2.47, whereas for brittle elemental Si it is 1.49. The calculated B/G value for TiSi_2 from our GGA (LDA) calculation is 1.27 (1.13) and this is much lower than that of its constituent. This result suggests that TiSi_2 is rather brittle.

The directional bulk modulus for the single crystal is calculated and compared with the corresponding experimental polycrystalline values in Table IV. Equations (A2), (A3), and (A4) are exact for single crystals, but only valid as approximations for the polycrystals. Our calculated bulk modulus is found to be in good agreement with the one obtained from the experimental elastic constants of Nakamura.² However, comparing the experimental values of the single crystal directional bulk modulus with the experimental polycrystalline values obtained by Peun, Lauterjung and Hinze¹⁷ from high pressure x-ray diffraction measurements show a difference of 14%. One possible origin for the discrepancy is that

TABLE IV. The isotropic bulk modulus (B in Mbar) and its upper bound (B_{unrelax} in Mbar), bulk modulus along the orthorhombic crystallographic axes a , b , and c (B_a , B_b , and B_c) for TiSi_2 .

	B	B_{unrelax}	B_a	B_b	B_c
LDA	1.569	1.591	4.189	4.434	5.788
GGA	1.419	1.450	3.636	3.975	5.620
Exp. 1 ^a	1.468	1.509	3.671	4.123	6.017
Exp. 2 ^b	1.269		3.180	3.300	5.590
LDA (normalized)			3.387	3.584	4.679
GGA (normalized)			3.251	3.554	5.025
Exp. 1 (normalized)			3.173	3.564	5.202

^aFrom Peun, Lauterjung, and Hinze (see Ref. 20).

^bCalculated from the single crystal elastic constants of Nakamura (see Ref. 2).

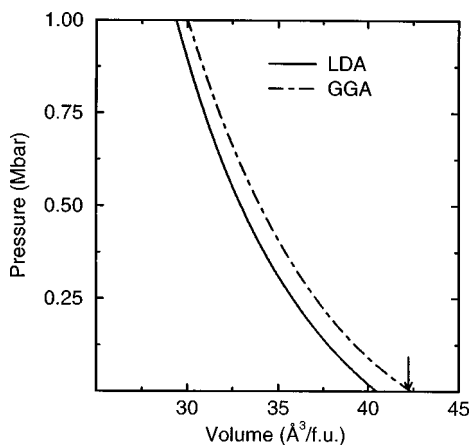


FIG. 6. Equation of state for TiSi_2 from LDA and GGA calculations. The arrow indicates the experimental equilibrium volume.

their isotropic bulk modulus was very much smaller than that obtained from Hill's average of bulk modulus given in Table III. Hence, we have normalized our linear bulk modulus using the experimental bulk modulus.¹⁷ The corresponding data are given in Table IV.

The bulk, shear, and Young's moduli of TiSi_2 given in Table III are substantially higher than those of the constituent elements and the average value based on the rule of mixtures. The large elastic modulus of TiSi_2 is due to stronger directional bonding between Si as well as that between Ti and Si. On the other hand, the Poisson's ratio for TiSi_2 is much smaller than those of the constituent elements and the average value based on the rule of mixtures. Poisson's ratio is associated with the volume change during uniaxial deformation. If $\nu=0.5$, no volume change occurs during elastic deformation. The low ν value for TiSi_2 means that a large volume change is associated with its deformation. In addition, Poisson's ratio provides more information about the characteristics of the bonding forces than any of the other elastic constants.²¹ It has been proved that $\nu=0.25$ is the lower limit for central-force solids and 0.5 is the upper limit, which corresponds to infinite elastic anisotropy.²² The low ν value (substantially smaller than 0.25) for TiSi_2 indicates that the interatomic forces in the compound are noncentral. In support of the above view point the ratios c_{23}/c_{44} , c_{31}/c_{55} , and c_{12}/c_{66} obtained from the Cauchy relations deviate considerably from unity.

A. Equation of state studies

We have also calculated the equation of state (the pressure versus volume) by taking the volume derivative of the fitted total energy obtained from our LDA and GGA calcu-

lation; the results are shown in Fig. 6. We cannot compare them with the experiment since there are no high pressure data available for TiSi_2 . The bulk modulus and its pressure derivative for TiSi_2 , obtained by fitting the total energy curve to the universal equation of state,²³ yield 1.565 Mbar and 4.4 in our LDA calculations and 1.392 Mbar and 4.3 in our GGA calculation, respectively. These bulk modulus values are found to be in good agreement with the one obtained from the calculated single crystal elastic constants [using Eq. (A1)] given in Table IV, namely 1.569 and 1.419 Mbar.

V. ELASTIC ANISOTROPY

It is well known that microcracks are induced in ceramics owing to the anisotropy of the coefficient of thermal expansion as well as elastic anisotropy.²⁴ Hence it is important to calculate elastic anisotropy in structural intermetallics in order to understand these properties and hopefully find mechanisms which will improve their durability. Essentially all the known crystals are elastically anisotropic, and a proper description of such an anisotropic behavior has, therefore, an important implication in engineering science as well as in crystal physics. The shear anisotropic factors provide a measure of the degree of anisotropy in the bonding between atoms in different planes. The shear anisotropic factor for the $\{100\}$ shear planes between the $\langle 011 \rangle$ and $\langle 010 \rangle$ directions is

$$A_1 = \frac{4c_{44}}{c_{11} + c_{33} - 2c_{13}}. \quad (17)$$

For the $\{010\}$ shear planes between $\langle 101 \rangle$ and $\langle 001 \rangle$ directions it is

$$A_2 = \frac{4c_{55}}{c_{22} + c_{33} - 2c_{23}}, \quad (18)$$

and for the $\{001\}$ shear planes between $\langle 110 \rangle$ and $\langle 010 \rangle$ directions it is

$$A_3 = \frac{4c_{66}}{c_{11} + c_{22} - 2c_{12}}. \quad (19)$$

The shear anisotropic factors obtained from our theoretical studies along with the ones obtained from the experimental values are given in Table V. For an isotropic crystal the factors A_1 , A_2 , and A_3 must be one, while any value smaller or greater than unity is a measure of the degree of elastic anisotropy possessed by the crystal. It is interesting to note that the experimental shear anisotropic factors show a higher degree of anisotropy than the values obtained from LDA as well as GGA calculations (Table V). This shows that theory

TABLE V. The shear anisotropic factors A_1 , A_2 , A_3 , and A_G (in %), A_B (in %) and compressibility anisotropy factors A_{Ba} and A_{Bc} for TiSi_2 obtained from LDA, GGA calculations, and the experimental study.

	A_1	A_2	A_3	A_G	A_B	A_{Ba}	A_{Bc}
LDA	0.718	0.651	0.933	2.909	0.677	0.944	1.305
GGA	0.766	0.743	0.938	3.005	1.069	0.914	1.413
Exp. ^a	0.688	0.539	0.811	3.565	1.394	0.890	1.459

^aCalculated from the single crystal elastic constants of Nakamura (see Ref. 2).

predicts a lower anisotropy in the bonding charge density between the different planes than the experiment.

In cubic crystals, the linear bulk modulus is the same for all directions and hence, the shear anisotropy alone is sufficient to describe the elastic anisotropy. On the other hand, for orthorhombic crystals, the elastic anisotropy arises from the anisotropy of the linear bulk modulus in addition to the shear anisotropy. The anisotropies of the bulk modulus along the **a** axis and **c** axis with respect to the **b** axis can be written as

$$A_{B_a} = \frac{B_a}{B_b} = \alpha$$

and (20)

$$A_{B_c} = \frac{B_c}{B_b} = \frac{\alpha}{\beta},$$

respectively. It is interesting to note that the quantities α and β defined in the Appendix couple to the elastic anisotropy of the crystal when approximating the polycrystalline sample with a single crystal. The above-mentioned shear and compressibility anisotropy factors were calculated and are listed in Table V. Note that for these parameters, a value of one indicates elastic isotropy and any departure from one corresponds to a degree of elastic anisotropy. Alternatively, Chung and Buessem introduced²⁵ a concept of percent elastic anisotropy which is a measure of elastic anisotropy possessed by the crystal under consideration. The percentage anisotropy in compressibility and shear are defined as

$$A_B = \frac{B_V - B_R}{B_V + B_R}$$

and (21)

$$A_G = \frac{G_V - G_R}{G_V + G_R},$$

respectively, where B and G are the bulk and shear moduli, and the subscripts V and R represent the Voigt and Reuss bounds. For these two expressions, a value of zero represents elastic isotropy and a value of 1 (100%) is the largest possible anisotropy. The percentage of bulk and shear anisotropies are listed in Table V. Clearly, the calculated elastic constants exhibit less elastic anisotropy than the experimentally reported elastic constants.²

The above defined shear moduli and bulk moduli are not sufficient to describe the elastic behavior of a crystal completely. A surface construction that is useful in practice is

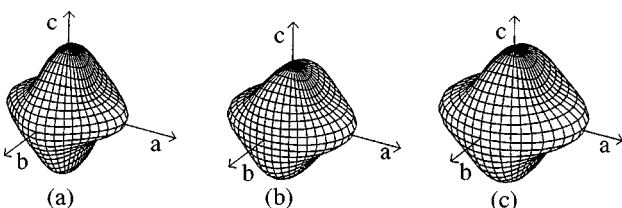


FIG. 7. Illustration of directional dependent Young's modulus of TiSi_2 : (a) calculated from LDA elastic constants, (b) from GGA elastic constants, and (c) from the experimental elastic constants of Nakamura (see Ref. 2).

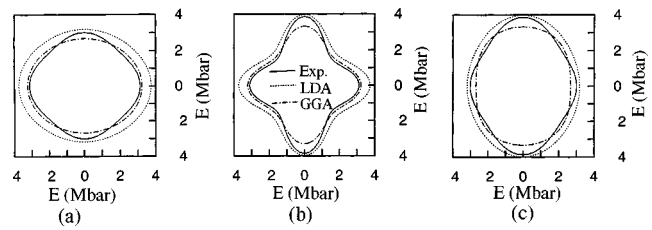


FIG. 8. Projections of the directional dependent Young's modulus in different planes for TiSi_2 . The continuous lines are obtained from the experimental elastic constants of Nakamura (see Ref. 2), the dot-dashed line represents the GGA results, and the dotted line represents the LDA result: (a) along the ab plane, (b) along the ac plane, and (c) along the bc plane.

one that shows the variation of Young's modulus with direction. The direction dependent Young's modulus (E) for orthorhombic crystals can be defined²⁶ as

$$\frac{1}{E} = l_1^4 + 2l_1^2 l_2^2 s_{12} + 2l_1^2 l_3^2 s_{13} + l_2^4 s_{22} + 2l_2^2 l_3^2 s_{23} + l_3^4 s_{33} + l_2^2 l_3^2 s_{44} + l_1^2 l_3^2 s_{55} + l_1^2 l_2^2 s_{66}, \quad (22)$$

where s_{ij} are the usual elastic compliance constants and l_1 , l_2 , and l_3 are the direction cosines in any arbitrary direction. From the above relation the estimated direction dependent Young's modulus for TiSi_2 , using the elastic compliance constant obtained from our LDA and GGA calculations and the experimental result,² are shown in Fig. 7. The elastic anisotropy in TiSi_2 is clearly visible from Fig. 7. It should be noted that the overall topology of the Young's modulus surface is similar in all three cases. However, due to the underestimation of the volume by LDA, it follows that the estimated Young's modulus in different directions is larger than those obtained from GGA calculation as well as from experimental studies. In order to have a better understanding of the origin of the changes in Young's modulus along different directions we have also given Young's modulus along the ab , ac , and cb planes in Fig. 8. From this figure one can see that both LDA and GGA predict that Young's modulus is more isotropic than that found experimentally.

The experimentally observed²⁷ anisotropy in the resistivity for different crystallographic orientations was found to be smaller than 20%. Our calculated anisotropy of Young's modulus along different crystallographic orientations is found to be higher than 40%. This result indicates that TiSi_2 is elastically more anisotropic than its electronic transport properties. The elastic constants c_{11} and c_{33} are important, among others, because they are related to the deformation behavior and atomic bonding characteristics of transition metal silicides. It can be seen from Table II that $c_{33} > c_{11}$ for TiSi_2 . The implication of this is that the atomic bonds along the $\{001\}$ planes between nearest neighbors are stronger than those along the $\{100\}$ plane. By considering the bulk modulus as a measure of the average bond strength and shear modulus as a measure of the resistance to a change in bond angle by an external force, Tanaka *et al.*²⁸ proposed that G/B represents the relative directionality of the bonding in the material. The value of G/B for TiSi_2 is larger than that of Ti and Si, indicating that the directionality of the bonding in TiSi_2 is stronger than that of its constituents.

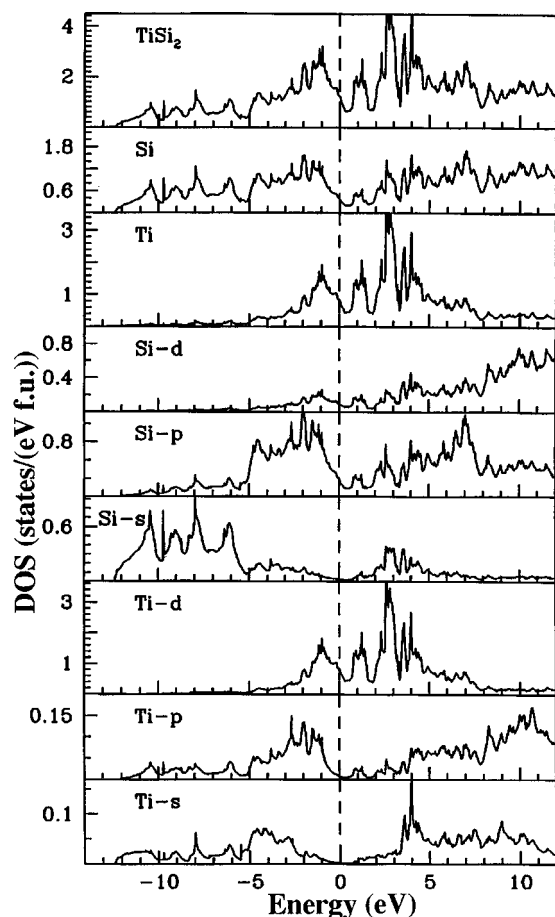


FIG. 9. Angular momentum and site decomposed electron density of states of TiSi_2 .

VI. CHEMICAL BONDING ANALYZED FROM CHARGE DENSITY AND DENSITY OF STATES STUDIES

The total, site and angular momentum decomposed DOS of TiSi_2 are shown in Fig. 9. The total DOS shows that there is a deep valley close to the Fermi level (E_F) and this valley is referred to as a pseudogap. This pseudogap indicates the presence of covalent bonding in TiSi_2 . Quite often the pseudogap separates the bonding states from the antibonding/nonbonding states. There exists a correlation between structural stability and the position of E_F with respect to the pseudogap.²⁹ From Fig. 9 we observe that the Fermi level falls below the pseudogap in TiSi_2 . This indicates that not all the bonding states are filled and some extra electrons are required to reach maximum stability in this compound. This may be the reason for the presence of an orthorhombic C49 metastable phase at low temperatures.

Considerable attention has been focused on TiSi_2 in order to understand its bonding properties.^{30,31} To gain more insight into the bonding behavior of TiSi_2 we have given the charge density contour plots of TiSi_2 in the 010 plane in Fig. 10. The interesting aspect of this figure is the presence of a strong directional bonding between the Si atoms. In this plane each face centered Ti atom is surrounded by six Si atoms. There is only a weak directional bonding between Ti and Si. The charge around the Ti sites is moved towards the Si atoms and this is consistent with the larger electronegativ-

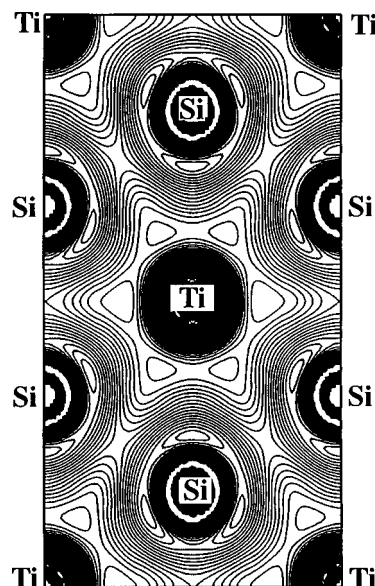


FIG. 10. The valence charge density for TiSi_2 in the 010 plane. 90 contours have been drawn between the charge distribution 0.01 and 0.1 electrons/ a.u.^3 .

ity of Si compared to Ti. Our site decomposed DOS shows that the density of states at the Fermi level is dominated by Ti d states. Even though considerable amount of Si s and p states are present in the occupied part of the DOS, their contribution at the Fermi level is very small. The DOS curves also show that the larger part of the broad Ti d DOS is above E_F . The overall topology of our DOS curves are found to be in good agreement with the X-ray photoemission spectrum.³⁰

As already mentioned the charge density contours in Fig. 10 show that there is a strong directional bonding between the Si atoms. Further, our angular momentum and site decomposed DOS given in Fig. 9 show that the Si $3s$ states are mixed with Si($3p$) states over the whole range of the conduction band, indicating large Si($3s$)–Si($3p$) hybridization. This observation is important for the bonding in TiSi_2 and is in agreement with the conclusion arrived from the soft X-ray emission spectroscopy (SXES) study.³² So far little attention has been given to understanding the role of Si($3d$) states on the chemical bonding in TiSi_2 . From the SXES study it was concluded³² that a finite amount of Si($3d$) states is present in the valence band. In order to confirm this we have also shown the Si($3d$) DOS in Fig. 9. From this figure it is clear that a considerable amount of Si($3d$) states is present in the energy region 0–5 eV below E_F in TiSi_2 .

The calculated value of $N(E_F)$ for TiSi_2 from our GGA treatment is 2.47 state/(eV cell). This value is found to be in good agreement with the value of 2.42 states/(eV cell) obtained from an linearly augmented plane wave (LAPW) calculation.³³ Recently Affronte *et al.*³⁴ estimated the renormalized electronic density of states at the Fermi level to be 2.85 states/(eV cell) using low temperature specific heat measurement. From this we calculate an electron–phonon mass enhancement factor of 0.152. This suggests a low value of electron–phonon coupling constant, which may explain why no superconductivity has been observed for TiSi_2 , al-

TABLE VI. The density (ρ in g/cm^3), longitudinal, transverse, average elastic wave velocity (v_l , v_s , v_m in m/s), and the Debye temperature from the average elastic wave velocity obtained from polycrystalline elastic modulus ($\theta_{D\rho}$ in K) and single crystal elastic constants (θ_{Ds} in K).

	ρ	v_l	v_s	v_m	$\theta_{D\rho}$	θ_{Ds}
LDA	4.2230	9028	5750	6321	788	775
GGA	4.0471	8694	5487	6038	742	722
Exp. ^a	4.0937	8629	5345	5894	727	700
Exp. ^b	664
Exp. ^c	560–588

^aCalculated from the single crystal elastic constants of Nakamura (see Ref. 2).

^bSpecific heat measurements by Affronte *et al.* (see Ref. 34).

^cSingle crystal resistivity measurements by Hirano and Kaise (see Ref. 40).

though superconductivity has been observed in structurally related systems like CoSi_2 , TaSi_2 , and NbSi_2 .

VII. CALCULATION OF DEBYE TEMPERATURE

As a fundamental parameter, the Debye temperature correlates with many physical properties of solids, such as specific heat, elastic constants, and melting temperature. At low temperatures the vibrational excitations arise solely from acoustic vibrations. Hence, at low temperatures the Debye temperature calculated from elastic constants is the same as that determined from specific heat measurements. One of the standard methods to calculate the Debye temperature (θ_D) is from elastic constant data, since θ_D may be estimated from the averaged sound velocity, v_m , by the equation³⁵

$$\theta_{D\rho} = \frac{h}{k} \left[\frac{3n}{4\pi} \left(\frac{N_A \rho}{M} \right) \right]^{1/3} v_m, \quad (23)$$

where h is Planck's constant, k is Boltzmann's constant, N_A is Avogadro's number, ρ is the density, M is the molecular weight and n is the number of atoms in the molecule. In Table VI the density of TiSi_2 obtained from the experimental and theoretical data is given. Because of the underestimated volume in LDA the calculated density is higher than the experimental value. The average wave velocity v_m in the polycrystalline material is approximately given by³⁵

$$v_m = \left[\frac{1}{3} \left(\frac{2}{v_l^3} + \frac{1}{v_t^3} \right) \right]^{-1/3}, \quad (24)$$

where v_l and v_t are the longitudinal and transverse elastic wave velocity of the polycrystalline material and are obtained (using the polycrystalline shear modulus G and the bulk modulus B) from Navier's equation as follows:³⁶

$$v_l = \left(\frac{B + \frac{4G}{3}}{\rho} \right)^{1/2}$$

and

$$v_t = \left(\frac{G}{\rho} \right)^{1/2}. \quad (25)$$

The θ_D can also be obtained from the average sound velocity obtained by integrating the elastic wave velocities over various directions of the single crystal from the c_{ij} using the following relation:³⁷

$$\theta_{Ds} = \frac{h}{k} \left(\frac{9N}{4\pi V} \right)^{1/3} \rho^{-1/2} a_0^{-1/3}, \quad (26)$$

where h , k , and ρ have the usual meaning described in Eq. (23), N is the number of atoms in one molecule, V is the volume of the unit cell, and a_0 is a function which represents the average velocity of elastic waves in different directions of the single crystal. Joardar *et al.*³⁷ derived the explicit expressions to calculate this function for orthorhombic crystals for ten different directions using

$$a_0 = [38976(f_A + f_B) + 15118f_C + 47628f_D + 38788(f_E + f_F) - 44352(f_G + f_H)]/105840,$$

where f_A , f_B , f_C , f_D , f_E , f_F , f_G , and f_H are the values of the function a_0 in the (100), (010), (001), (110), (011), (101), ($\sqrt{3}10$), ($1\sqrt{3}0$), ($01\sqrt{3}$), and ($10\sqrt{3}$) directions, respectively. These values can be obtained from the single crystal elastic constants using the explicit expressions for different directions given by Joardar *et al.*³⁷ The reliability of the calculated value of θ_{Ds} depends upon the number of directions considered in our calculations. Joardar *et al.*³⁷ showed that ten different directions give reasonably good values of the Debye temperature. Affronte *et al.*³⁴ estimated the Debye temperature of TiSi_2 from the low temperature specific heat measurements and the value given in Table VI is lower than the one obtained from the experimental as well as our theoretical elastic constants. By fitting the temperature dependence of the resistivity with a Bloch–Grüneisen curve, Thomas *et al.*²⁷ estimated a Debye temperature of 535 ± 10 K. It should be noted that the specific-heat measurements³⁸ in the temperature range 100–500 K gave an estimation of $\theta_D = 510$ K. From these results it is clear that the Debye temperature of TiSi_2 increases with decreasing temperature. This conclusion is consistent with the general behavior of a decreasing Debye temperature with increasing temperature in intermetallic compounds.³⁹ Further, only the acoustic branches of phonons are active at low temperatures and hence, the estimated θ_D from our elastic constants is valid for low temperatures. It is interesting to note that the Debye temperature obtained from Eq. (24) is closer to the experimental value than the one obtained often from Eq. (23) given in Table VI. From temperature dependent electrical resistivity measurement, Hirao and Kaise⁴⁰ found that the Debye temperature for TiSi_2 has a minimum value of 560 K along the (001) direction and a maximum value of 588 K along the (010) direction. It should be noted that the θ_D obtained from elastic constants is always higher than that obtained from electrical resistivity studies. The discrepancy may be partly ascribed to its temperature dependence.

VIII. CONCLUSIONS

We have used the FLMTO method to perform a set of first principles, self-consistent, total energy calculations to determine the equations of state and equilibrium structural

parameters of TiSi_2 in the orthorhombic C54 structure. The calculated lattice constants are in excellent agreement with the experimental data when we use the GGA for the exchange and correlation potential. We also calculated the strain energies for nine different distortions of TiSi_2 using LDA as well as GGA in the theoretically optimized crystal structure in order to calculate elastic constants. Overall the elastic constants obtained from the GGA calculations are found to be somewhat in better agreement with the experimental values than those obtained from LDA calculations. From the elastic constants, the bulk moduli along the crystallographic axes are calculated and are compared with experimental values. The comparison of directional dependent bulk modulus and Young's modulus obtained from the LDA and GGA calculations with experimental results show that the GGA considerably improves the elastic properties of TiSi_2 . Using Hill's approximation, the ideal polycrystalline aggregates bulk modulus, shear modulus, Young's modulus, and Poisson's ratio, are calculated. The Poisson's ratio of TiSi_2 was found to be lower than that of ordinary metals and alloys and this shows clear deviations from central forces in this material. We also discussed the chemical bonding in TiSi_2 through the angular momentum and site decomposed density of states, charge density analysis, and elastic anisotropy, of this material. From the theoretically obtained polycrystalline shear moduli and bulk moduli as well as the average elastic wave velocity over different directions, the Debye temperature was calculated and found to be in good agreement with the experimental values.

ACKNOWLEDGMENTS

The authors are thankful for financial support from the Swedish Natural Science Research Council and for support from the Materials Science Consortium No. 9. One of the authors, P.R. wishes to acknowledge L. Nordström for his many useful discussions in the course of this study. Part of the work was performed under the auspices of the U.S. Department of Energy.

APPENDIX: CALCULATION OF BULK MODULUS ALONG CRYSTALLOGRAPHIC AXES

From pressure dependent lattice parameter measurements it is easy to obtain the bulk modulus of a solid along different crystallographic axes. It is however simpler to calculate the bulk modulus along the crystallographic axes from the single crystal elastic constants. From elastic theory, by considering the definition of the bulk modulus where the strains perpendicular to the stress directions are all equal (the case of response to a hydrostatic pressure) one will arrive at

$$B_{\text{relax}} = \frac{\Lambda}{(1 + \alpha + \beta)^2}, \quad (\text{A1})$$

where $\Lambda = c_{11} + 2c_{12}\alpha + c_{22}\alpha^2 + 2c_{13}\beta + c_{33}\beta^2 + 2c_{23}\alpha\beta$. For tetragonal and hexagonal crystals $\alpha = 1$ and for cubic crystals $\alpha = \beta = 1$. For orthorhombic crystals α and β can be defined as

$$\alpha = \frac{(c_{11} - c_{12})(c_{33} - c_{13}) - (c_{23} - c_{13})(c_{11} - c_{13})}{(c_{33} - c_{13})(c_{22} - c_{12}) - (c_{13} - c_{23})(c_{12} - c_{23})},$$

and

$$\beta = \frac{(c_{22} - c_{12})(c_{11} - c_{13}) - (c_{11} - c_{12})(c_{23} - c_{12})}{(c_{22} - c_{12})(c_{33} - c_{13}) - (c_{12} - c_{23})(c_{13} - c_{23})}.$$

The single crystal isotropic bulk modulus (B_{relax}) obtained from Eq. (A1) is the same as the one obtained from experimental pressure studies on a single crystal, where the relaxation of a/b and c/b as a function of pressure is considered. Interestingly, this value is exactly the same as the one obtained from the Reuss average i.e., the lower bound of the bulk modulus) given in Table III. In general, to minimize the amount of computations, the bulk modulus of the orthorhombic system will be obtained by varying the volume for fixed a/b and c/b values. This will always give an upper bound to the bulk modulus (B_{unrelax}). This value can be obtained from Eq. (A1) by substituting $\alpha = \beta = 1$. The B_{unrelax} value obtained from Eq. (A1), using the above procedure, is given in Table IV and is exactly the same as one obtains from Voigt averages given in Table III. The bulk modulus along the \mathbf{a} , \mathbf{b} and \mathbf{c} axis are defined as

$$B_a = a \frac{dP}{da} = \frac{\Lambda}{1 + \alpha + \beta}, \quad (\text{A2})$$

$$B_b = b \frac{dP}{db} = \frac{B_a}{\alpha}, \quad (\text{A3})$$

$$B_c = c \frac{dP}{dc} = \frac{B_a}{\beta}, \quad (\text{A4})$$

where α and β are defined as the relative change of the \mathbf{b} and \mathbf{c} axis as a function of the deformation of the \mathbf{a} axis. Using the above relations, the linear bulk modulus can be obtained from our calculated single crystal elastic constants.

¹M. E. Fine, L. D. Brown, and H. L. Marcus, *Scr. Metall.* **18**, 951 (1984); R. L. Fleischer, Proceedings of the International Symposium on Intermetallic Compounds (JIMIS-6), edited by O. Izumi (Japan Institute of Metals, Sendai, Japan, 1991), pp. 157–163.
²M. Nakamura, *Metall. Trans. A* **25A**, 331 (1993).
³S. F. Pugh, *Philos. Mag.* **45**, 823 (1954).
⁴M. Nakamura, *Intermetallic Compounds: Principles*, edited by J. H. Westbrook and R. L. Fleischer (Wiley, New York, 1994), Vol. 1, p. 873.
⁵M. J. Mehl, B. M. Klein, and D. A. Papaconstantopoulos, in *Intermetallic Compounds: Principles*, edited by J. H. Westbrook and R. L. Fleischer (Wiley, New York, 1994), Vol. 1, p. 195.
⁶C. L. Fu and M. H. Yoo, *Philos. Mag. Lett.* **58**, 199 (1988); J. Chen, L. L. Boyer, H. Krakauer, and M. J. Mehl, *Phys. Rev. B* **37**, 3295 (1988); J. M. Wills, O. Eriksson, P. Söderlind, and A. M. Boring, *Phys. Rev. Lett.* **68**, 2802 (1992); P. Söderlind, O. Eriksson, J. M. Wills, and A. M. Boring, *Phys. Rev. B* **48**, 5844 (1993); N. E. Christensen, *Solid State Commun.* **49**, 701 (1984); **50**, 177 (1984); M. Dacorogna, J. Ashkenasi, and M. Peter, *Phys. Rev. B* **26**, 1527 (1982); D. Iotova, N. Kioussis, and S. P. Lim, *ibid.* **54**, 14413 (1996); G. Bihlmayer, R. Eibler, and A. Necker, *ibid.* **50**, 13113 (1994); X.-Q. Guo, R. Podloucky, and A. J. Freeman, *J. Mater. Res.* **6**, 324 (1991); M. J. Mehl, *Phys. Rev. B* **47**, 2493 (1993).
⁷M. J. Mehl, J. E. Osburn, D. A. Papaconstantopoulos, and B. M. Klein, *Phys. Rev. B* **41**, 10311 (1990); C. L. Fu and M. H. Yoo, *Philos. Mag.* **62**, 159 (1990); C. L. Fu, *J. Mater. Res.* **5**, 971 (1990); M. Alouani, R. C. Albers, and M. Methfessel, *Phys. Rev. B* **43**, 6500 (1991).
⁸L. Fast, J. M. Wills, B. Johansson, and O. Eriksson, *Phys. Rev. B* **51**, 17431 (1995); P. Söderlind, J. A. Moriarty, and J. M. Wills, *ibid.* **53**, 14063 (1996).

- ⁹W. Jeitschko, *Acta Crystallogr., Sect. B: Struct. Crystallogr. Cryst. Chem.* **33**, 2347 (1977).
- ¹⁰J. Mass, G. Bastin, F. van Loo, and R. Metselaar, *Z. Metallkd.* **75**, 140 (1984).
- ¹¹R. Rosenkranz and G. Frommeyer, *Z. Metallkd.* **83**, 9 (1992).
- ¹²J. M. Wills (unpublished); J. M. Wills and B. R. Cooper, *Phys. Rev. B* **36**, 3809 (1987); D. L. Price and B. R. Cooper, *ibid.* **39**, 4945 (1989).
- ¹³D. C. Wallace, *Thermodynamics of Crystals* (Wiley, New York, 1972).
- ¹⁴J. P. Perdew, J. A. Chevary, S. H. Vosko, K. A. Jackson, M. R. Pederson, and D. J. Singh, *Phys. Rev. B* **46**, 6671 (1992).
- ¹⁵O. K. Andersen, *Phys. Rev. B* **12**, 3060 (1975); H. L. Skriver, *The LMTO Method* (Springer, Berlin, 1984).
- ¹⁶D. J. Chadi and M. L. Cohen, *Phys. Rev. B* **8**, 5747 (1973); S. Froyen, *ibid.* **39**, 3161 (1989).
- ¹⁷T. Peun, J. Lauterjung, and E. Hinze, *Nucl. Instrum. Methods Phys. Res. B* **97**, 487 (1995).
- ¹⁸W. Voigt, *Lehrbuch der Kristallphysik* (Taubner, Leipzig, 1928).
- ¹⁹A. Reuss, *Z. Angew. Math. Mech.* **9**, 55 (1929).
- ²⁰R. Hill, *Proc. Phys. Soc. London* **65**, 350 (1952).
- ²¹W. Koster and H. Franz, *Metall. Rev.* **6**, 1 (1961).
- ²²M. H. Ledbetter, *Materials at Low Temperatures*, edited by R. P. Reed and A. F. Clark (American Society for Metals, Metals Park, OH, 1983), p. 1.
- ²³P. Vinet, J. H. Rose, J. Ferrante, and J. R. Smith, *J. Phys.: Condens. Matter* **1**, 1941 (1989).
- ²⁴V. Tvergaard and J. W. Hutchinson, *J. Am. Chem. Soc.* **71**, 157 (1988).
- ²⁵D. H. Chung and W. R. Buessem, in *Anisotropy in Single Crystal Refractory Compound*, edited by F. W. Vahldiek and S. A. Mersol (Plenum, New York, 1968), Vol. 2, p. 217.
- ²⁶J. F. Nye, *Physical Properties of Crystals* (Oxford University Press, Oxford, 1985).
- ²⁷O. Thomas, R. Madar, J. P. Senateur, and O. Laborde, *J. Less-Common Met.* **136**, 175 (1987).
- ²⁸K. Tanaka, K. Okamoto, H. Inui, Y. Minonishi, M. Yamaguchi, and M. Koiwa, *Philos. Mag. A* **73**, 1475 (1996).
- ²⁹J.-H. Xu, T. Oguchi, and A. J. Freeman, *Phys. Rev. B* **35**, 6940 (1987); J.-H. Xu and A. J. Freeman, *ibid.* **40**, 11927 (1989); **41**, 12553 (1990); *J. Mater. Res.* **6**, 1188 (1991); P. Ravindran, G. Subramoniam, and R. Asokamani, *Phys. Rev. B* **53**, 1129 (1996).
- ³⁰P. J. W. Weijs, M. T. Czyzyk, J. C. Fuggle, W. Speier, D. D. Sarma, and K. H. J. Buschow, *Z. Phys. B* **78**, 423 (1990).
- ³¹A. Franciosi and J. H. Weaver, *Surf. Sci.* **132**, 324 (1983); J. H. Weaver, A. Franciosi, and V. L. Moruzzi, *Phys. Rev. B* **29**, 3293 (1984).
- ³²N. Zhou, M. Hiri, M. Kusaka, M. Iwami, and H. Nakamura, *Jpn. J. Appl. Phys., Part 1* **29**, 2014 (1990).
- ³³L. F. Matheiss and J. C. Hensel, *Phys. Rev. B* **39**, 7754 (1989).
- ³⁴M. Affronte, O. Laborde, J. C. Lasjaunias, U. Gottlieb, and R. Madar, *Phys. Rev. B* **54**, 7799 (1996).
- ³⁵O. L. Anderson, *J. Phys. Chem. Solids* **24**, 909 (1963).
- ³⁶E. Schreiber, O. L. Anderson, and N. Soga, *Elastic Constants and their Measurements* (McGraw-Hill, New York, 1973).
- ³⁷P. Joardar, S. Chatterjee, and S. Chakraborty, *Indian J. Phys., A* **54A**, 433 (1980).
- ³⁸W. K. Sylla, S. E. Stillman, M. S. Sabella, and E. J. Cotts, *J. Appl. Phys.* **76**, 2752 (1994).
- ³⁹P. Bujard and E. Walker, *Solid State Commun.* **39**, 667 (1981).
- ⁴⁰T. Hirano and M. Kaise, *J. Appl. Phys.* **68**, 627 (1990).